Estimation of Vehicle States Using a Cascaded Hybrid Estimation Method

Marvin Glomsda[a], Hendrik Tino Prümer[b] and Philipp Maximilian Sieberg[c]
Chair of Mechatronics, University of Duisburg-Essen, Lotharstr. 1, Duisburg, Germany

Keywords: Hybrid State Estimation, Hybrid Estimation Methods, Cascaded Hybrid Estimation Method, Vehicle State Estimation.

Abstract: Three models using a cascaded hybrid estimation method with physical models of different degrees of accuracy are evaluated for their overall precision and interpretability. Hybrid estimation methods hereby denote methods concatenating the properties of physics-based models and artificial neural networks for the purpose of improved state estimation. Cascaded hybrid estimation methods are a subtype of these methods, combining a physical model and an artificial neural network in a way that one acts as the input of the other. In this publication the result of a physical model is fed into a neural network to improve the estimation quality. It can be shown that the degree of accuracy of the physical model has an influence on the overall estimation quality, with more accurate physical models yielding better results, but less accurate models can provide a more significant improvement through the artificial neural network. This is likely due to the larger residual error that can be used to train the artificial neural network.

1 INTRODUCTION

The requirements for vehicle state estimation continue to rise. Therefore, new approaches, so-called hybrid methods, have been developed, that combine a physics-based model with an artificial neural network (Sieberg et al., 2019). As the development of artificial neural networks and such hybrid methods continues, it is important to examine different approaches. Various methods, shown in (Gräber et al., 2018; Kim et al., 2021; Li et al., 2021; Wu et al., 2024), could be interpreted as cascaded hybrid estimation models, which thus far has not been extensively tested for vehicle dynamics. The information flow and the decision-making of artificial neural networks tends to be non-transparent, as their structure tends to be complex, especially for demanding estimation tasks. This could also be the case with a cascaded hybrid method, as all information is passed through the artificial neural network. The EU Artificial Intelligence Act (Smuha, 2025) shows that the first legal requirements are already being placed on artificial neural networks and their operation. The interpretability and therefore traceability of the decision-making of an artificial neural network are also regulated. Security, reliability, transparency, traceability, and documentation are focussed and various operators are held responsible to ensure these aspects (Smuha, 2025). Interpretation methods are necessary for transparency and traceability. Some of these methods are listed in (Carvalho et al., 2019; Linardatos et al., 2020; Zhang et al., 2021), and offer options for interpreting artificial neural networks.

2 METHODOLOGY

This publication aims to investigate if cascaded hybrid estimation models offer an attractive opportunity to enhance state estimation based solely on physical modelling. To validate this approach, physical models with three different degrees of accuracy are used and combined with a subsequent artificial neural network. All three estimation tasks are chosen from the automotive field, however the

[a] https://orcid.org/0009-0003-2821-0253
[b] https://orcid.org/0009-0007-2349-6474
[c] https://orcid.org/0000-0002-4017-1352

Glomsda, M., Prümer, H. T. and Sieberg, P. M.
Estimation of Vehicle States Using a Cascaded Hybrid Estimation Method.
DOI: 10.5220/0013646200003970
In *Proceedings of the 15th International Conference on Simulation and Modeling Methodologies, Technologies and Applications (SIMULTECH 2025)*, pages 126-134
ISBN: 978-989-758-759-7; ISSN: 2184-2841

findings from the investigation should be applicable over a wide variety of application fields. For the estimation tasks within this publication a simulation environment is used, which combines IPG CarMaker and MATLAB & Simulink in a co-simulation. The application examples chosen for this investigation are the estimation of the side-slip angle, the yaw rate, and the tyre load of the front left tyre. For proper investigation, the degree of accuracy was varied for the physical models utilised for each state estimation. Table 1 gives an overview over the physical models used and their respective degree of accuracy.

Table 1: Overview of degree of accuracy for chosen state estimation parameters, derived from (Schramm et al., 2018).

Parameter	Physical Model	Degree of Accuracy
Side-slip angle	Double-track model	High
Yaw rate	Equilibrium of momentum of double-track model	Medium
Tyre load (front left)	Quarter-vehicle model	Low

By using models with different accuracy, it can be investigated if the estimation quality can be increased by cascading physical models with a subsequent artificial neural network. To assess the quality of the output, three main performance indices are used, root mean square error, permutation feature importance, and local interpretable model-agnostic explanation. The root mean square error takes into account the ground truth of IPG CarMaker. Permutation feature importance and local interpretable model-agnostic explanation, on the other hand, serve to evaluate how interpretable the state estimation is. The permutation feature importance is a measure for global interpretability (Molnar, 2020), while the local interpretable model-agnostic does the same locally (Ribeiro et al., 2016). This is based on the concern of having all information processed through the artificial neural network and the estimated state using no measured quantity directly. To evaluate how beneficial the integration of the artificial neural network within the hybrid method is to the overall state estimation, the output of each physical model is evaluated as well.

3 MODELLING

In this section, the used methods will be described. First, the overall structure will be presented, followed by its subparts, namely the three different physical models and the artificial neural network. Lastly, the driving manoeuvres, used to generate the data for the training of the artificial neural network and the overall validation, will be presented.

3.1 Overall Structure

As described in the Methodology section, a cascaded hybrid state estimation approach shall be used for this study. This approach is implemented for each estimated parameter individually. The basic structure of the artificial neural network remains unchanged for the different estimation tasks. The applied physical models are presented in Table 1. The IPG CarMaker environment, a multi-body vehicle simulation validated for example by (Cheok et al., 2023), provides the input data into the models as well as the ground truth values for the estimation tasks. The overall structure is depicted in Figure 1. IPG Carmaker provides sensor signals, which are used as inputs into the physical model as well as the artificial neural network for estimating the target quantities. These estimations are then compared to the ground truth quantities, which are also provided by IPG Carmaker. Thus, the estimation of the physical model can be compared against the estimation by the hybrid method.

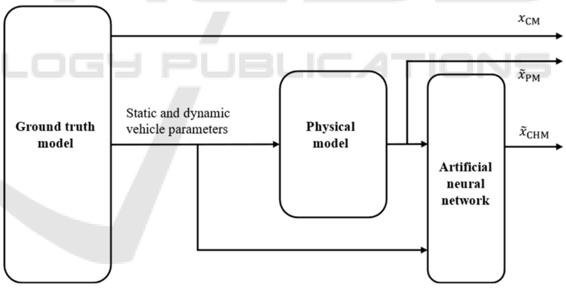

Figure 1: Overall structure of the simulation environment.

3.2 Model for Side-Slip Angle Estimation

A twin-track model as described in (Schramm et al., 2018) is used as the basis for the physical model that estimates the side-slip angle. All necessary arguments for this model are taken from the IPG CarMaker environment, except for the vehicle velocity, the acceleration as well as the side-slip angle and its derivative. These quantities are representing inner states of the physical model. Vehicle acceleration and side-slip angle derivative are both integrated and the fed back to the system, respectively. Both values are initialised with zero, as the vehicle starts each simulation run in straight standstill. Constants are the vehicle mass and gravitational acceleration. In contrast the chassis forces for each suspended wheel, the vehicle roll and pitch angle, the wind force acting on the entire vehicle, and the tyre velocities are dynamic input quantities provided by IPG CarMaker. Figure 2 depicts this approach.

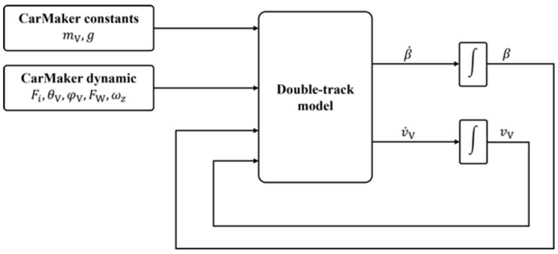

Figure 2: Implementation of the physical model for side-slip angle estimation.

The side-slip angle β is used as the single output of the twin-track model and fed into the artificial neural network alongside longitudinal, lateral, and vertical acceleration, roll, pitch, and yaw angle, vehicle velocity, steering angle of the front wheels, and the simulated time. This is depicted in Figure 3. The structure of the artificial neural network will be described in section 3.5.

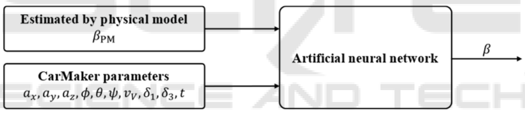

Figure 3: Implementation of the artificial neural network for side-slip angle estimation.

3.3 Model for Yaw Rate Estimation

As the degree of accuracy for the yaw rate estimation shall be lower compared to the task of estimating the side-slip angle, the momentum equilibrium of the twin-track model is selected for this purpose instead of the direct use of the twin-track model. The time integration needed for the calculation of the yaw rate with this approach leads to a summation of the integration error, as the yaw rate is not fed back into the model. The chassis forces for each suspended wheel and the steering angle for both front wheels serve as the dynamic inputs for this model, while wheelbase, the longitudinal position of the centre of gravity, front and rear track width and the moment of inertia of the vehicle are constant. This structure is visualised in Figure 4.

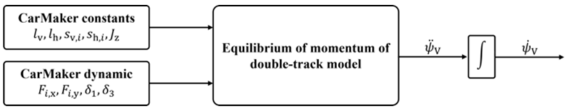

Figure 4: Implementation of the physical model for yaw rate estimation.

As shown in Figure 5, the artificial neural network for the estimation of the yaw rate uses the same inputs from IPG CarMaker as the one for the side-slip angle estimation. In addition, the physical model provides the estimation of the yaw rate as an input.

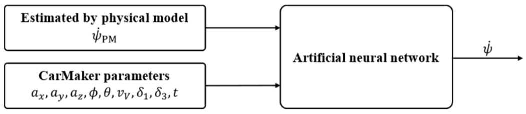

Figure 5: Implementation of the artificial neural network for yaw rate estimation.

3.4 Model for Tyre Load Estimation

For the estimation of the tyre load, a quarter-car model is used for the physical part of the hybrid estimation. This model can be represented by a linear state-space representation. The structure of the quarter-car model is based on the equations from (Schramm et al., 2018). The constants such as tyre stiffness, spring and damper constants, tyre mass and body mass of the front left vehicle body are taken from the IPG CarMaker environment, as shown in Figure 6. The damping of the tyre is assumed to be zero. Other constants used for this estimation are the inertia of rotation around the tyre's rotation axis and the distances to the vehicle's centre of gravity. The excitation caused by the road surface is dynamically provided by the IPG CarMaker environment for the contact point of the front left tyre and fed to the system.

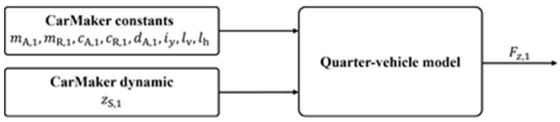

Figure 6: Implementation of the physical model for tyre load estimation.

Alongside the estimated tyre load of the front left tyre, the artificial neural network is given longitudinal, lateral, and vertical acceleration, pitch angle, road excitation, simulated time, and the lengths of spring, damper, and distance of wheel carrier to centre of gravity of the front left as well as the rear left tyre, as depicted in Figure 7.

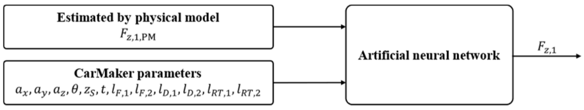

Figure 7: Implementation of the artificial neural network for tyre load estimation.

3.5 Structure of Artificial Neural Network

An identical base structure was chosen for the artificial neural networks of all three estimation models. As the deviation between the outputs of each physical and the ground truth model may incorporate nonlinearities and represents a time-series prediction problem, an artificial neural network based on long short-term memory (LSTM) cells was chosen. (Zhang et al., 2024) showed that such networks can be used for the modelling of vehicle dynamics.

The concrete network structure used for this study is shown in Figure 8 and starts with a sequence input layer that feeds the time series data to two LSTM layers. To omit overfitting issues, a dropout layer is integrated after each LSTM layer, deactivating LSTM cells randomly during the training process. Lastly, the information passes through one fully-connected layer, one rectified linear unit layer, and one single fully-connected termination neuron, as only one parameter is to be estimated by each artificial neural network. A regression layer is added to allow a continuous estimation.

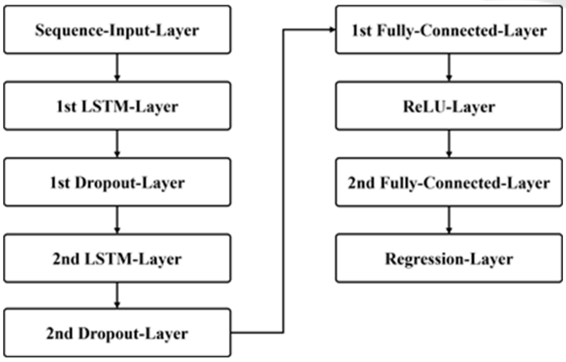

Figure 8: Structure of the artificial neural network used for all three models presented in this publication.

Of the generated training data, 70 % are used for the training of the artificial neural network itself, while the other 30 % are used for in-training validation. The data are based on the simulations of the driving manoeuvres presented in section 3.6. No experimental data were used to train the models.

A hyperparameter optimisation was carried out for each artificial neural network individually. The results of this hyperparameter optimisation are shown in Table 2 for all three artificial neural networks.

Table 2: Results of hyperparameter optimisation.

Hyper-parameter	Range	Side-Slip Angle	Yaw Rate	Tyre Load
Sequence length	50 – 200	137	170	184
Hidden layers (LSTM 1)	32 – 128	122	83	124
Dropout 1	0.1 – 0.5	0.1088	0.4454	0.3965
Hidden layers (LSTM 2)	32 – 128	110	106	120
Dropout 2	0.1 – 0.5	0.3164	0.2441	0.4834
Neurons of fully connected layer 1	10 – 100	61	19	16
Batch size	50 – 200	90	53	69
Gradient threshold	0.5 – 5	1.9771	1.6865	4.4373
Initial learning rate	10^{-2} – 10^{-4}	0.0028	0.0060	0.0041
Learning rate drop period	5 – 50	44	33	22
Learning rate drop factor	0.1 – 0.9	0.1887	0.4875	0.6515
Validation frequency	50 – 200	151	117	55
L2 regularisation	10^{-2} – 10^{-6}	$1.7509 \cdot 10^{-6}$	$1.8262 \cdot 10^{-6}$	$1.2816 \cdot 10^{-6}$

For this purpose, the sequence length of the input and the LSTM network configuration, such as the size of the hidden layer, fully connected layer, and the values of the dropout layer are chosen as hyperparameters. The Adam optimizer is used for this purpose. The number of epochs is limited to 50 for the Bayesian optimisation method (Frazier, 2018). Furthermore, the batch size, gradient threshold, initial learning rate, learning rate drop period, learning rate drop factor, validation frequency (with validation patience of 100), and the use of L2 regularisation are defined as hyperparameters. The hyperparameters for the three neural networks are approximated after 30 iterative steps of the Bayesian optimisation method with the search for the lowest root mean square error of the normalised validation data. The results of this optimisation do not use the minimum or maximum values of the specified intervals. L2 regularisation is required for each neural network presented here.

3.6 Manoeuvres for Data Generation

According to the estimation tasks, the same manoeuvres were used to obtain the data used to train, validate, and test the hybrid estimation of the side-slip angle and the yaw rate. For those manoeuvres, attention was paid to high excitation of the estimation quantities. Two different slaloms and one double lane change setup were used here with multiple velocities used for all of them. Table 3 gives an overview over the exact manoeuvre setups. All simulation outputs were updated every 0.01 s for the duration of the manoeuvres. The measure given for each slalom determines the distance between consecutive cones of the slalom. The double lane change used for training data generation was the one from the General German Automobile Club (ADAC) (Diehm et al., 2013), while the double lane change according to ISO 3888-1 (Standardization, 2018) with an entry velocity of 90 km/h was used to generate the test data for the estimation of side-slip angle and yaw rate, which is listed in Table 4.

Table 3: Overview of all manoeuvres used for training data generation in this study.

Manoeuvre	**Variable**	**Range**	**Interval**
Side-slip angle and yaw rate estimation			
Slalom 18 m	Velocity	20 - 60 km/h	20 km/h
Slalom 36 m	Velocity	20 - 100 km/h	20 km/h
Double lane change (ADAC)	Velocity	20 - 100 km/h	20 km/h
Tyre load estimation			
Speed bump	Velocity	5 - 11 km/h	2 km/h
	Bump height	0 - 8 cm	2 cm

To generate the training data for the tyre load estimation, a speed bump setup with three subsequent speed bumps of equal height was used. Vehicle velocity and height of the bumps were varied according to Table 3.

The test data in this case was obtained with a track consisting of three bumps of different height and a vehicle velocity of 6 km/h. The heights of the bumps were set to 1 cm for the first, 7 cm for the second, and 5 cm for the third bump. Table 4 shows the setups used for test data generation.

Table 4: Overview of the manoeuvres used for test data generation in this study.

Manoeuvre	**Variable**	**Value**
Side-slip angle and yaw rate estimation		
Double lane change (ISO)	Entry velocity	90 km/h
Tyre load estimation		
Speed bump	Velocity	6 km/h
	Bump height	1 cm (first bump) 7 cm (second bump) 5 cm (third bump)

These relatively simple manoeuvres were chosen on purpose to enable potential reasoning within the interpretability part of each estimation evaluation.

4 RESULTS

In this section, the results achieved by the hybrid method for the different estimation tasks will be presented. The structure follows the sequence established in Table 1, starting with the results for the side-slip angle estimation, followed by the results for the yaw rate estimation, and completed by the results for the estimation of the tyre load. Each estimation approach is discussed individually here, as a comparative conclusion follows in the next section.

4.1 Results for Side-Slip Angle Estimation

First of all, a visual comparison is presented in Figure 9. As it can be seen in this figure, the direct output of the physical model matches the ground truth curve better than the output of the artificial neural network that was supposed to correct any remaining deviations and increase the accuracy.

This can also be seen in the root mean square error that calculates to 0.0004 for the output of the physical model and to 0.0023 for the output of the artificial neural network.

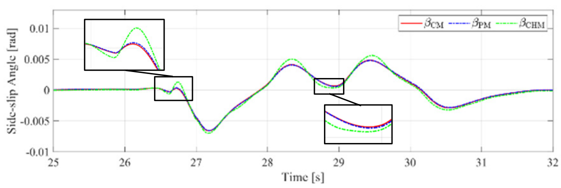

Figure 9: Visual comparison between ground truth (red), physical model (blue) and cascaded hybrid state estimation (green) for side-slip angle estimation.

The permutation feature importance yields a very conclusive result for the artificial neural network used as part of the cascaded hybrid state estimation for the estimation of the side-slip angle. The artificial neural network relies nearly entirely on the estimated side-slip angle provided by the physical model. However, the slight impact of the other inputs seems to worsen the estimation instead of improving it. Table 5 shows the permutation feature importance for all inputs of this artificial neural network.

Table 5: Permutation feature importance for artificial neural network used for side-slip angle estimation.

Feature	Relative Importance
β_{PM}	199.2931 %
a_y	0.6652 %
a_x	0.6643 %
θ_{V}	0.6259 %
ϕ_{V}	0.3648 %
δ_1	0.3200 %
δ_3	0.2561 %
v_{V}	0.0098 %
ψ_{V}	0.0040 %
t	-0.0054 %
a_z	-0.2826 %

This assumption can be supported by the local interpretable model-agnostic explanation which was assessed exemplarily for the deviation highlighted on the left side of Figure 9. This analysis shows that at that exact deviation the calculation of the artificial neural network was dominated by the yaw rate among other inputs while the estimation of the physical model was completely neglected in this moment, as can be seen in Table 6.

Table 6: Local interpretable model-agnostic explanation for the left deviation highlighted in Figure 9.

Feature	Model Coefficient
ψ_{V}	0.0023
θ_{V}	0.0012
a_x	0.0012
δ_1	0.0011
δ_3	0.0011
a_z	0.0008
ϕ_{V}	0.0007
a_y	0.0007
t	0.0000
v_{V}	0.0000
β_{PM}	0.0000

4.2 Results for Yaw Rate Estimation

Figure 10 shows the great influence of the integration error obtained when using the physical model described in subsection 3.3 without any correction. The output of the physical model was corrected for a static offset.

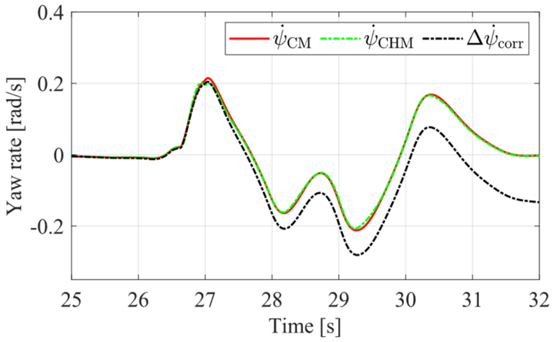

Figure 10: Estimated yaw rate for test data: Ground truth model (red), estimation by the physical model (black, corrected for static offset) and by cascaded hybrid state estimation (green) for yaw rate estimation.

This drastic improvement is also supported by the root mean square error, which is 0.0657 for the physical model after the offset correction and 0.0041 for the output of the artificial neural network on the test data, more than one order of magnitude better.

The permutation feature importance is much more balanced for the yaw rate estimation compared to the side-slip angle estimation. Longitudinal acceleration has the highest importance, followed by the roll angle. The results for all inputs can be seen in Table 7.

Table 7: Permutation feature importance for artificial neural network used for yaw rate estimation.

Feature	Relative Importance
a_x	88.8793 %
θ_{V}	56.1443 %
a_y	20.0293 %
ϕ_{V}	13.1013 %
δ_1	8.0284 %
δ_3	6.4708 %
v_{V}	0.7281 %
t	-0.0033 %
$\dot\psi_{\mathrm{PM}}$	-0.2019 %
a_z	-8.8256 %

As no large deviations can be observed, the local interpretable model-agnostic explanation, performed on the first peak visible in Figure 10, yields similar results as the permutation feature importance. These results are shown in Table 8.

Table 8: Local interpretable model-agnostic explanation for first peak visible in Figure 10.

Feature	Model Coefficient
a_x	0.0205
θ_{V}	0.0156
ϕ_{V}	0.0145
a_y	0.0141
δ_1	0.0117
a_z	0.0116
δ_3	0.0104
$\dot{\psi}_{\mathrm{PM}}$	0.0008
t	0.0000
v_{V}	0.0000

4.3 Results for Tyre Load Estimation

For a proper visual examination, Figure 11 shows each bump of the test manoeuvre separately. At the excitations at about 14 s, 23 s, and 32 s, the direct effect of each bump can be seen, while at the excitations at about 16 s, 25 s, and 34 s, the effect of the rear wheel hitting the same bump is visible. It becomes apparent that the quarter-car model is unable to replicate these second excitations. The cascaded hybrid state estimation, while being worse at the estimation of the exact values of the single peaks, can replicate the effect caused by the rear wheel.

When looking at the root mean square error, this results in an improvement from 0.0389 for the physical model to 0.0174 for the output of the artificial neural network.

The permutation feature importance shows the highest influence for the vertical acceleration of the vehicle, followed by the elevation of the vehicle's centre of gravity, the estimated tyre load of the physical model and the length of the wheel carrier of the rear left wheel. Table 9 shows the permutation feature importance of all inputs of the artificial neural network used for tyre load estimation of the front left tyre.

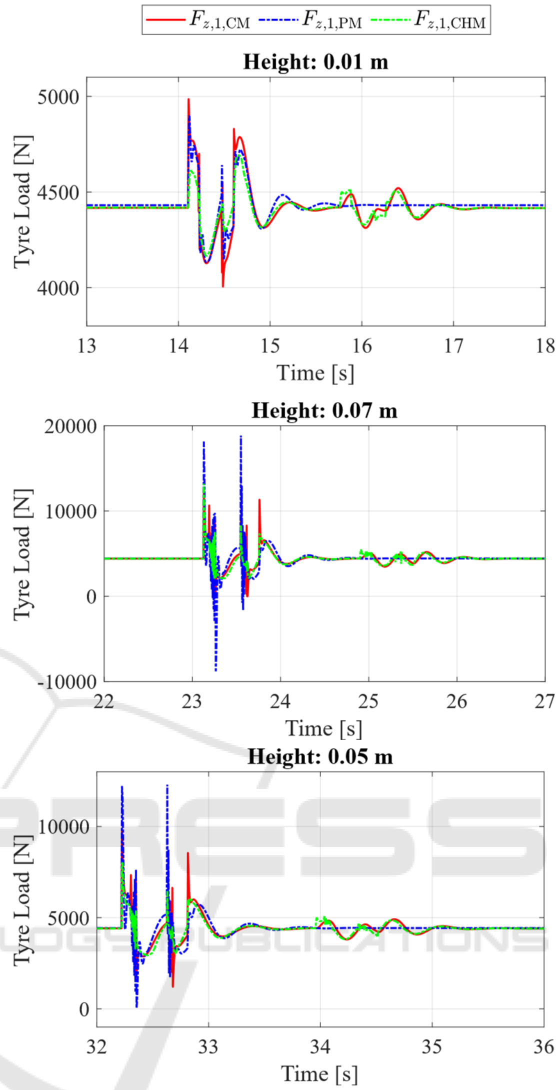

Figure 11: Estimated tyre load for front left wheel: Ground truth model (red), estimation by the physical model (blue) and by cascaded hybrid state estimation (green), portrayed separately for each bump of the test manoeuvre.

The local interpretable model-agnostic explanation, calculated for the first peak portrayed in Figure 11, shows a similar result as the permutation feature importance for this model, with an even higher reliance on the estimated tyre load of the physical model. All results of this evaluation are shown in Table 10.

Table 9: Permutation feature importance for artificial neural network used for tyre load estimation of front left tyre.

Feature	Relative Importance
a_z	335.9293 %
z_S	149.7106 %
$F_{z,1,\mathrm{PM}}$	93.0265 %
$l_{\mathrm{RT},2}$	63.9848 %
a_x	23.8769 %
$l_{\mathrm{F},1}$	19.2051 %
$l_{\mathrm{D},1}$	14.9819 %
θ_V	13.2897 %
$l_{\mathrm{RT},1}$	10.9508 %
v_V	3.6284 %
$l_{\mathrm{D},2}$	3.1289 %
$l_{\mathrm{F},2}$	1.6099 %
a_y	0.5285 %
t	-0.0026 %

Table 10: Local interpretable model-agnostic explanation for first peak shown in Figure 11.

Feature	Model Coefficient
$F_{z,1,\mathrm{PM}}$	93.7598
a_z	61.6276
z_S	48.2679
v_V	44.3520
a_x	31.3720
$l_{\mathrm{D},1}$	7.9202
t	6.5219
$l_{\mathrm{D},3}$	5.7612
a_y	0.0000
θ_V	0.0000
$l_{\mathrm{F},1}$	0.0000
$l_{\mathrm{F},2}$	0.0000
$l_{\mathrm{RT},1}$	0.0000
$l_{\mathrm{RT},2}$	0.0000

5 CONCLUSION

The results for the root mean square error are ambiguous, as Table 11 shows. For the side-slip angle estimation, the root mean squared error increases for the hybrid method compared to the sole use of the physical model, but at a very low level compared to the other two estimation tasks. Yaw rate and tyre load estimation show an improvement in estimation quality.

Table 11: Overview of root mean square error for chosen state estimation parameters.

Parameter	Physical Model	Cascaded Hybrid State Estimation
Side-slip angle	0.0004	0.0023
Yaw rate	0.0657	0.0041
Tyre load	0.0389	0.0174

The permutation feature importance shows a different dependency of the artificial neural networks on the parameters estimated by the physical models. While the artificial neural network for the estimation of the side-slip angle relies nearly completely on this input, the artificial neural network used for the estimation of the yaw rate near-completely omits the use of the input provided by the physical model. The artificial neural network of the model estimating the tyre load uses the value estimated by the connected physical model as one of the most important inputs, while also relying strongly on some of the other inputs provided.

These findings lead to the conclusion that the artificial neural network as part of a cascaded hybrid state estimation needs a certain room for improving the estimation to be able to train properly. This is an interesting finding as normalised values were used for the training of the artificial neural networks. But it is reasonable to assume that the small deviation remaining after the physical model for the side-slip angle estimation might have been incidental rather than being related to any of the other inputs provided to the artificial neural network in this specific case.

6 OUTLOOK

One evaluation parameter currently not analysed, is the computational effort needed to carry out the cascaded hybrid state estimation models. This could be achieved by comparing the effect of the different simulation stages (ground truth model, with added physical model, and with added cascaded hybrid method) on the central processing unit. The cascaded hybrid models obtained in this study should also be tested with more difficult test manoeuvres on their robustness. Lastly, a comparison to other (hybrid) state estimation methods, including Kalman filter based methods, should be undertaken to find the optimal structure for a given estimation task.

The original contributions presented in this study are included in the article. Further inquiries can be directed to the corresponding author.

REFERENCES

Carvalho, D. V., Pereira, E. M., & Cardoso, J. S. (2019). Machine learning interpretability: A survey on methods and metrics. Electronics, 8(8), 832.

Cheok, J. H., Lee, K. O., Aparow, V. R., Amer, N., Peter, C., & Magaswaran, K. (2023). Validation of scenario-based virtual safety testing using low-cost sensor-based instrumented vehicle. Journal of Mechanical Engineering and Sciences, 9520-9541.

Diehm, G., Maier, S., Flad, M., & Hohmann, S. (2013). Online identification of individual driver steering behaviour and experimental results. 2013 ieee international conference on systems, man, and cybernetics,

Frazier, P. I. (2018). Bayesian optimization. In Recent advances in optimization and modeling of contemporary problems (pp. 255-278). Informs.

Gräber, T., Lupberger, S., Unterreiner, M., & Schramm, D. (2018). A hybrid approach to side-slip angle estimation with recurrent neural networks and kinematic vehicle models. IEEE Transactions on Intelligent Vehicles, 4(1), 39-47.

Kim, D., Kim, G., Choi, S., & Huh, K. (2021). An integrated deep ensemble-unscented Kalman filter for sideslip angle estimation with sensor filtering network. IEEE Access, 9, 149681-149689.

Li, W., Zhang, J., Ringbeck, F., Jöst, D., Zhang, L., Wei, Z., & Sauer, D. U. (2021). Physics-informed neural networks for electrode-level state estimation in lithium-ion batteries. Journal of Power Sources, 506, 230034.

Linardatos, P., Papastefanopoulos, V., & Kotsiantis, S. (2020). Explainable ai: A review of machine learning interpretability methods. Entropy, 23(1), 18.

Molnar, C. (2020). Interpretable machine learning. Lulu. com.

Ribeiro, M. T., Singh, S., & Guestrin, C. (2016). " Why should i trust you?" Explaining the predictions of any classifier. Proceedings of the 22nd ACM SIGKDD international conference on knowledge discovery and data mining,

Schramm, D., Hiller, M., & Bardini, R. (2018). Vehicle dynamics. Modeling and Simulation. Berlin, Heidelberg, 2nd Edition.

Sieberg, P. M., Blume, S., Harnack, N., Maas, N., & Schramm, D. (2019). Hybrid state estimation combining artificial neural network and physical model. 2019 IEEE Intelligent Transportation Systems Conference (ITSC),

Smuha, N. A. (2025). Regulation 2024/1689 of the Eur. Parl. & Council of June 13, 2024 (Eu Artificial Intelligence Act). International Legal Materials, 1-148.

Standardization, I. O. f. (2018). ISO 3888 ‑ 1: 2018 Passenger cars−Test track for a severe lane ‑ change manoeuvre−Part 1: Double lane ‑ change. In.

Wu, M., Wang, Y., Zhang, Y., & Li, Z. (2024). Physics-Informed Neural Network for Mining Truck Suspension Parameters Identification. Advanced Vehicle Control Symposium,

Zhang, Y., Huang, Y., Deng, K., Shi, B., Wang, X., Li, L., & Song, J. (2024). Vehicle Dynamics Estimator Utilizing LSTM-Ensembled Adaptive Kalman Filter. IEEE Transactions on Industrial Electronics.

Zhang, Y., Tiňo, P., Leonardis, A., & Tang, K. (2021). A survey on neural network interpretability. IEEE Transactions on Emerging Topics in Computational Intelligence, 5(5), 726-742.